THE STRUCTURAL DESIGN OF TALL AND SPECIAL BUILDINGS
Struct. Design Tall Spec. Build. (2007)
Published online in Wiley Interscience (www.interscience.wiley.com). **DOI**: 10.1002/tal.368

PROS AND CONS OF MULTISTORY RC TUNNEL-FORM (BOX-TYPE) BUILDINGS

EROL KALKAN[1]* AND S. BAHADIR YÜKSEL[2]
[1] *California Geological Survey, Sacramento, CA, USA*
[2] *Department of Civil Engineering, Selcuk University, Konya, Turkey*

SUMMARY

Tunnel-form structural systems (i.e., box systems), having a load-carrying mechanism composed of reinforced concrete (RC) shear walls and slabs only, have been prevailingly utilized in the construction of multistory residential units. The superiority of tunnel-form buildings over their conventional counterparts stems from the enhanced earthquake resistance they provide, and the considerable speed and economy of their construction. During recent earthquakes in Turkey, they exhibited better seismic performance in contrast to the damaged condition of a number of RC frames and dual systems (i.e., RC frames with shear wall configurations). Thus the tunnel-form system has become a primary construction technique in many seismically active regions. In this paper, the strengths and weaknesses of tunnel-form buildings are addressed in terms of design considerations and construction applications. The impacts of shear wall reinforcement ratio and its detailing on system ductility, load-carrying capacity and failure mechanism under seismic forces are evaluated at section and global system levels. Influences of tension/compression coupling and wall openings on the response are also discussed. Three-dimensional nonlinear finite element models, verified through comparisons with experimental results, were used for numerical assessments. Findings from this projection provide useful information on adequate vertical reinforcement ratio and boundary reinforcement to achieve enhanced performance of tunnel-form buildings under seismic actions. Copyright © 2007 John Wiley & Sons, Ltd.

1. INTRODUCTION

A recent trend in the building industry in Turkey, as well as in many countries with increasing city populations, is toward utilizing the tunnel-form (shear wall dominant) construction system for development of multistory residential units. This has been driven basically by the need to construct earthquake-resistant multistory reinforced concrete (RC) buildings with considerable ease, speed and economy.

The tunnel-form system is an industrialized construction technique in which structural walls and slabs are cast (*in situ*) simultaneously using steel forms composed of vertical and horizontal panels set at right angles. Figure 1 portrays the typical tunnel-form building construction and special formwork system. To expedite the construction, non-structural components such as facade walls, stairs and chimneys are commonly produced as prefabricated elements. Tunnel-form buildings generally have a symmetrical configuration in horizontal and vertical planes (see Figure 1) that enables continuous flow of construction and better quality assurance.

Besides the constructive advantages, tunnel-form buildings provide superior seismic performance compared to conventional RC frame and dual systems, which suffered significant damage and total collapse in many regions during recent devastating earthquakes in Turkey (1999: Mw 7·4 Kocaeli, Mw 7·2 Duzce; and 2004: Mw 6·5 Bingol). In the aftermath of these events, the superior performance

*Correspondence to: Erol Kalkan, California Geological Survey, 801K Street, Mail Stop 13-35, Sacramento, CA 95814-3500, USA. E-mail: Erol.kalkan@conservation.ca.gov

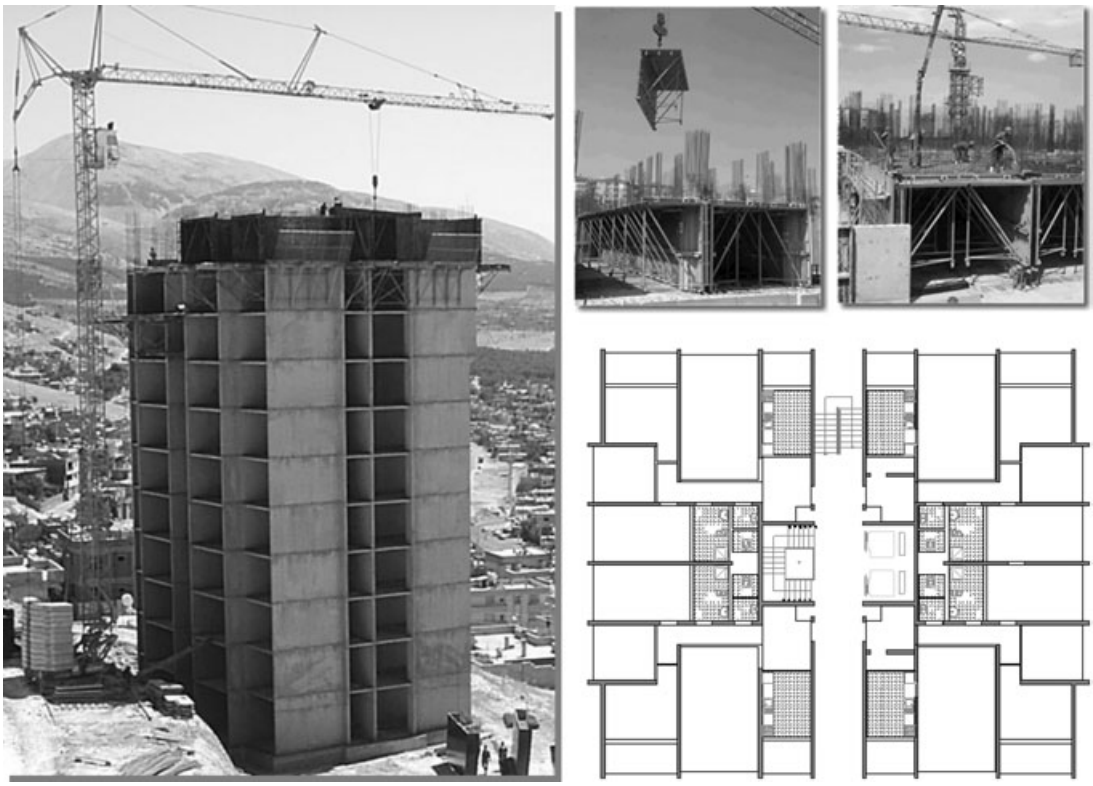

Figure 1. Multistory tunnel building construction system and typical symmetrical story plan. Note: thick lines in plan indicate shear walls

of tunnel-form buildings stimulated extensive use of this construction system for rehabilitation projects. Not only in Turkey, but also in many other countries prone to seismic risk, tunnel-form buildings have gained increasing popularity. In contrast, current seismic codes and provisions (e.g., IBC 2000; TSC, 1998; UBC, 1997) do not include specific guidelines for the earthquake-resistant design of tunnel-form buildings. Therefore, in practical applications, there has been an attempt toward implementing current design procedures primarily established for conventional RC frame-type and dual systems (i.e., structural systems having RC frames and shear wall configurations) into the design of tunnel-form buildings. However, recent studies show that empirical equations given in current design provisions (e.g., IBC, 2000; TSC, 1998; UBC, 1997) yield inaccurate estimates of fundamental period and result in erroneous computation of earthquake design forces when they are used blindly for tunnel-form buildings (e.g., Lee *et al.*, 2000; Balkaya and Kalkan, 2003a, 2004a; Ghrib and Mamedov, 2004). In addition, modern design guidelines for traditional RC buildings are not adequate to account for interactions of thinner shear wall and slab configurations as the common components of the tunnel-form system. Detailed evaluation of the response modification factor (i.e., R-factor) for tunnel-form buildings is also imperative (Balkaya and Kalkan, 2004a).

Due to such limitations, careless implementation of existing guidelines in tunnel-form building design may result in severe consequences. One such example is an eight-story shear wall dominant building (El-Faro building) which was heavily damaged during the 1985 Chile earthquake due to a flexure-triggered brittle mechanism. Such a failure mechanism is not routinely considered during seismic design (Wood *et al.*, 1991), and was experimentally shown to be a possible failure mechanism

DOI: 10.1002/tal

for tunnel-form buildings if vertical reinforcement of shear walls is designed and detailed improperly (Yüksel and Kalkan, 2007). Therefore, the main objective in advancing understanding of the structural behavior of tunnel-form buildings should be to improve the rationale of design. To this purpose, this paper addresses pros and cons of tunnel-form buildings in terms of their design considerations and construction applications. The impacts of shear wall vertical reinforcement and boundary reinforcement ratio on system ductility, load-carrying capacity and failure mechanism are carefully examined, and the effects of shear wall openings and tension/compression coupling on the lateral response are also highlighted. Nonlinear analyses on finite element (FE) models at global system level supported by moment–curvature analyses at section level are used to perform comprehensive numerical assessments. In order to represent nonlinear behavior and failure mechanism adequately, FE models are verified with the results of experimental studies conducted on three-dimensional (3D) scaled tunnel-form building specimens. Based on the information gained from numerical projections, design recommendations are presented at the end.

2. BRIEF DESCRIPTION OF EXPERIMENTAL STUDY

The experimental study, reported in Yüksel and Kalkan (2006), was initiated to obtain a better understanding of the 3D behavior of tunnel-form buildings under lateral loads. To this aim, four-story (1/5 scale) H-shape building specimens were tested under quasi-static reversed cyclic loading. Test specimens (so-called SP1 and SP2) were purposely detailed and constructed to reflect common practice in Turkey; therefore a minimum amount of mesh reinforcement (i.e., ratio of shear wall vertical reinforcement to wall nominal section area, $\rho_s = 0{\cdot}0015$) was utilized without accommodating boundary reinforcement in the shear walls (explained in detail later). Figure 2 demonstrates the test set-up for SP1 and SP2 loaded respectively along weak and strong axes at their roof levels. The experimental results showed that lightly reinforced structural walls of tunnel-form buildings with low axial stress may exhibit brittle flexural failure under cyclic loading. The brittle failure takes place due to rupture in longitudinal reinforcement with no crushing of concrete.

3. NONLINEAR FINITE ELEMENT MODELING

3D nonlinear FE models representative of test specimens (i.e., SP1 and SP2) were created using the general-purpose FE program, DIANA (TNO DIANA, 2004). The specimens were modeled using

Figure 2. Test set-up for specimen SP1 (loading along weak axis) and SP2 (loading along strong axis)

DOI: 10.1002/tal

eight-noded brick elements. A 4×4 gauss integration scheme in more than 13 000 elements was used. The models had fixed supports at foundation level, consistent with the experimental study. In FE models, the governing nonlinear phenomena in the ultimate limit state were cracking and crushing of concrete and the plastic behavior of reinforcement steel. The FE models allowed us to evaluate stress and deformations more comprehensively within a parametric framework; thereby a better understanding of the behavior of specimens during loading to failure was achieved. The assumptions made for modeling the concrete and reinforcement steel together with validation of FE models are explained in the following sub-sections.

3.1 Concrete material model

Behavior of concrete was idealized using a constitutive model based on nonlinear fracture mechanics. A crack model, having opening/closing and rotating capabilities based on the coaxial stress–strain concept, whereby the stress–strain relationships were evaluated in the principal directions of the strain vector, was employed. This constitutive model is based on the uniaxial stress–strain relationship describing tensile and compressive behavior where the stress is directly related to the total strain. Therefore, the approach is conceptually similar to hypoelasticity in which the loading and unloading are following the same stress–strain path (Takacs and Kanstad, 2000). The compression behavior of concrete was modeled using an unconfined concrete model proposed by Popovics (1973) and modified by Thorenfeldt *et al.* (1987). The tension stiffening of concrete was considered as a linear ascending curve up to cracking limit, and the tension softening portion of the stress–strain curve was based on the model proposed by Hordijk (1991), which utilizes *mode-I* fracture energy (G_f), ultimate tensile strength (f_t) and crack bandwidth (h_{cr}) to compute the maximum crack opening (w_u). This model results in a crack stress equal to zero at an ultimate crack strain (ε_u^{cr}). The crack bandwidth was computed based on the FE mesh dimensions. The corresponding concrete stress–strain relationship in compression and tension is shown in Figure 3(a) and (b), respectively. A constant shear retention factor (β-factor) to account for the degradation in shear stiffness after crack initiation (Figure 3c) was utilized as 0·1 based on verification studies. Poisson's ratio for concrete was taken as 0·20. Cracking of concrete was considered using a constant stress cut-off criterion, meaning that, once the maximum principal tensile stress reaches the tensile strength, independent of the other principal stresses, a crack is initiated perpendicular to the principal stress. The orientation of the crack is then stored and the material response perpendicular to the crack path is determined based on the stress–strain relation for the cracked material volume (Johansson, 2000).

3.2 Reinforcement steel material model

The constitutive behavior of the reinforcing steel was modeled using the Von-Mises plasticity model with an associated flow law and isotropic strain hardening. A smeared reinforcement model was utilized to simulate the reinforcement mesh. The smeared reinforcement model was treated as an equivalent uniaxial layer of material at the appropriate depth and smeared out over the element as several orthotropic layers. Transferring the strength and stiffness of the reinforcement directly into the concrete elements, this model is the easiest to implement, particularly for the modeling of mesh reinforcement. Since the slip between reinforcement and surrounding concrete was small enough for the test specimens, a perfect bond was assumed and steel nodes were rigidly attached to concrete element nodes. Stress–strain behavior of the steel was modeled using a bilinear relationship. The parameters of models were calibrated to test data provided by Yüksel and Kalkan (2006). The material properties and stress–strain relationship for reinforcing steel are presented in Figure 3(d).

DOI: 10.1002/tal

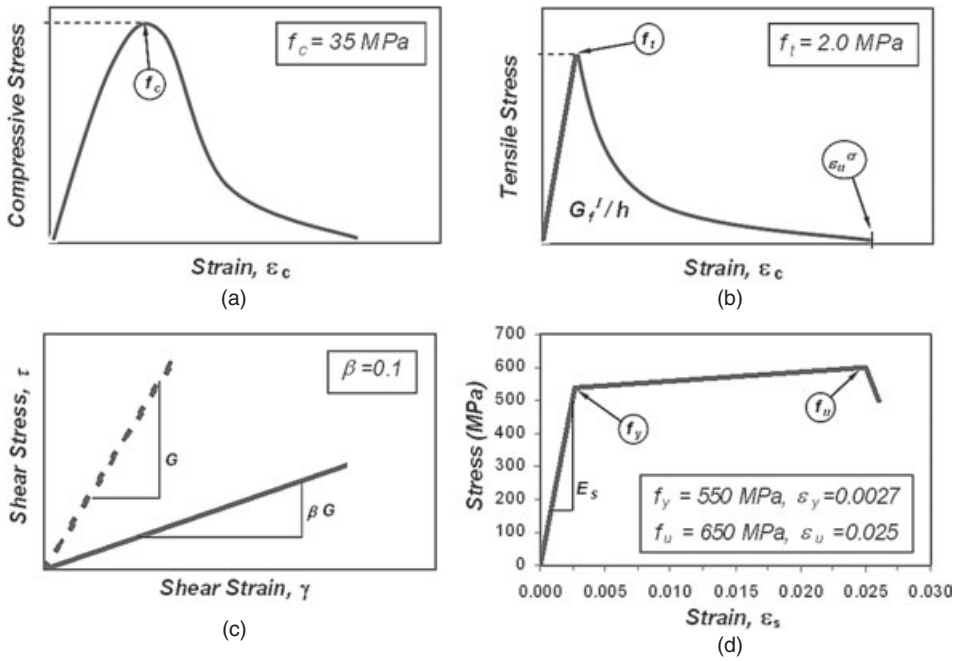

Figure 3. Concrete and steel nonlinear material models: (a) unconfined concrete model; (b) nonlinear tension-softening model; (c) shear retention; (d) reinforcement steel model

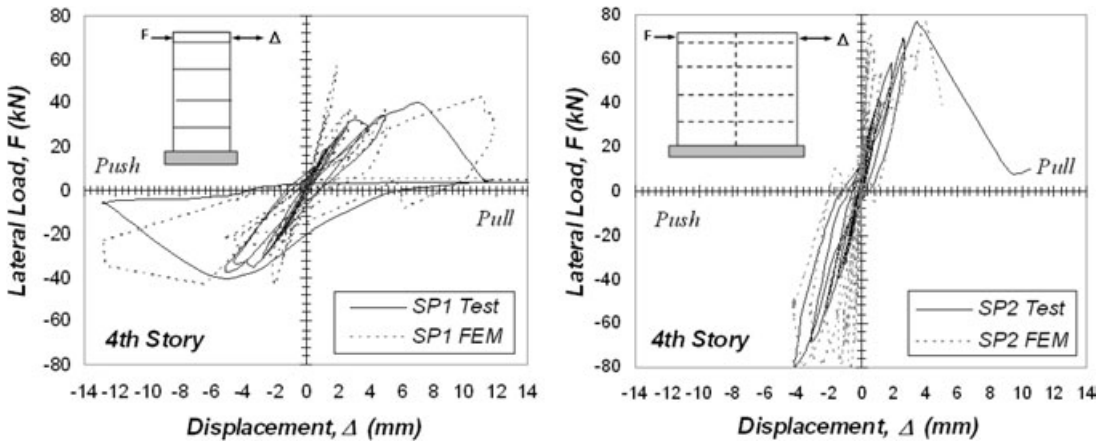

Figure 4. Comparison of computed (FEM) and experimental (test) cyclic response curves

3.3 Experimental validation of FE models

The experimental data reported in Yüksel and Kalkan (2006) were used for verification of simulated inelastic behavior. For that purpose, FE models were analyzed under similar cyclic loading conditions applied to test specimens (SP1 and SP2). Among different iteration schemes (e.g., Newton–Raphson) the BFGS (Broyden–Fletcher–Goldfarb–Shanno) scant stiffness method (see Bathe. 1996) was found to be more stable to achieve the convergence criterion specified as energy norm at each increment (an energy tolerance of 0·01% was used). The load versus deflection curves and cracking patterns shown

DOI: 10.1002/tal

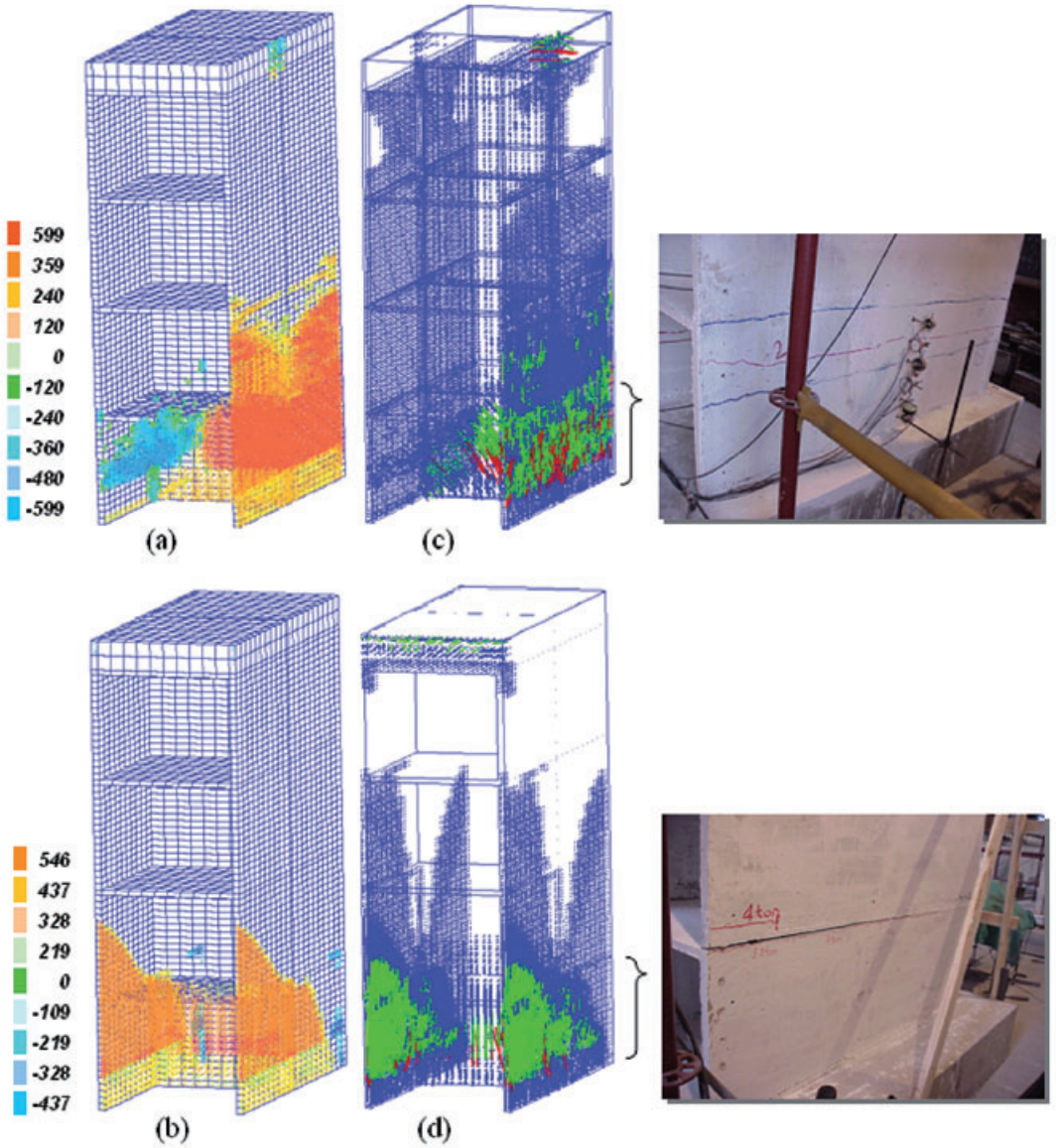

Figure 5. (a, b) Stress concentration on longitudinal bars at failure. Note: yield strength of steel is 540 MPa; negative sign indicates compression. (c, d) Comparison of computed and experimental damage patterns

in Figures 4 and 5 were used to determine the capabilities of the analytical models to replicate the observed 3D behavior. The results of FE analyses generally corresponded reasonably with the results of experiments; load versus displacement curves of the analytical study adequately overlapped the experimental results, and cracking patterns obtained were also well captured at the maximum load level. The models were found to be numerically stable. Despite some discrepancies, the overall good correlation between the experimental findings and numerical results enhanced the reliability of the analytical models.

DOI: 10.1002/tal

4. EFFECTS OF SHEAR WALL REINFORCEMENT ON BEHAVIOR

In order to investigate the effects of shear wall vertical reinforcement ratio (i.e., area of total vertical reinforcement divided by nominal section area) on global system response and failure mechanism, a parametric study, in which the wall vertical reinforcement ratio was varied from 0·0015, 0·003, and 0·006 to 0·01, was conducted. For that purpose, four different FE models were subjected to separate pushover analyses considering two orthogonal loading directions (i.e., along weak and strong axes). Pushover analyses were performed using invariant inverted triangle loading pattern. Gravity load was applied gradually and sustained prior to a displacement control incremental lateral loading. The first outcomes of the pushover analyses were the capacity curves represented as the total base shear versus roof displacement. In the first phase of evaluation, FE models were pushed to the same target displacements along weak and strong axes individually. These target displacements correspond to failure limits of the test specimens (i.e., SP1 and SP2) having the minimal vertical shear wall reinforcement ratio of 0·0015. In this way, we were able to examine the remedial effects of increasing reinforcement ratio on the inelastic behavior, lateral load-carrying capacity and prevention of premature brittle failure. Figure 6 shows the respective capacity curves obtained from models having various shear wall

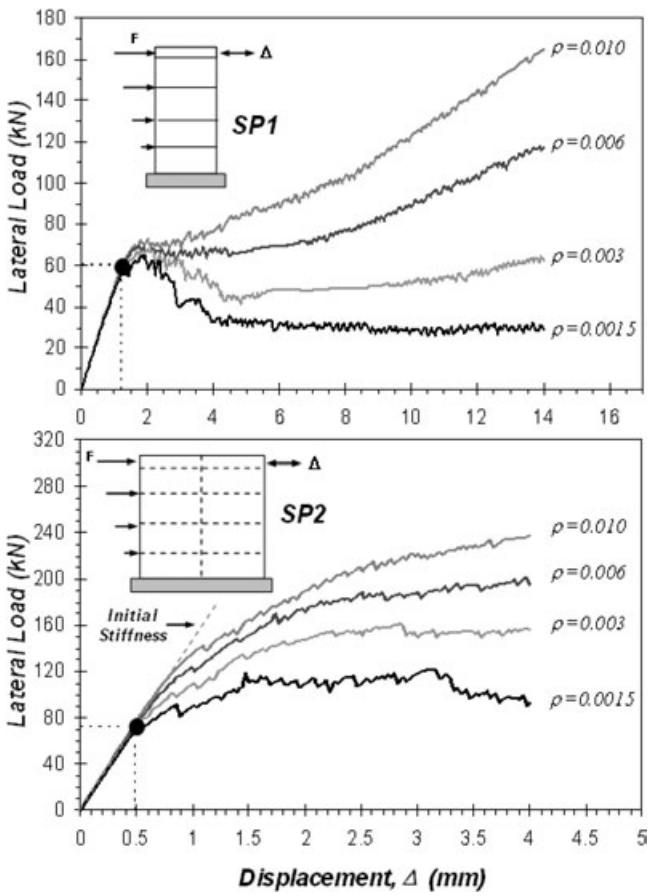

Figure 6. Variation lateral load capacity of SP1 and SP2 with change in shear wall reinforcement ratio. Note: abscissa and ordinates of the two figures are different

DOI: 10.1002/tal

reinforcement ratios. For SP1, significant load-carrying capacity was achieved by increasing the reinforcement ratio. Peak load capacity reached more than five times that of the model when reinforcement ratio was increased from 0·0015 to 0·01. Loading along the strong axis (SP2) resulted in somewhat less lateral load-carrying capacity compared to SP1. Similarly, increase in reinforcement ratio to 0·01 for SP2 yielded better system performance. In this case, up to three times larger lateral load-carrying capacity was obtained compared to SP2 having 0·0015 reinforcement ratio. While the system global yield point was similar for SP1, the yield point for SP2 shifted to larger values as the reinforcement ratio was increased. As compared to the brittle failure mechanism of SP1 and SP2 with 0·0015 reinforcement ratio, system behavior became more ductile as the reinforcement ratio was increased.

In the second phase of evaluation, FE models having a reinforcement ratio of 0·01 were pushed to their failure limits and the corresponding capacity curves are compared in Figure 7 against benchmark models having a reinforcement ratio of 0·0015. Owing to fact that the global failure mechanism is controlled by the reinforcement ratio in thin shear walls, increase in reinforcement ratio altered the system failure mechanism from brittle mode (with 0·0015) to a more desirable ductile mode (with 0·01). For both SP1 and SP2, 0·01 reinforcement ratio resulted in around 1·5 times larger system ductility by allowing further cracking of concrete and preventing sudden rupture of reinforcement. At the failure of SP1 (with a reinforcement ratio of 0·01), longitudinal bars ruptured before crushing of

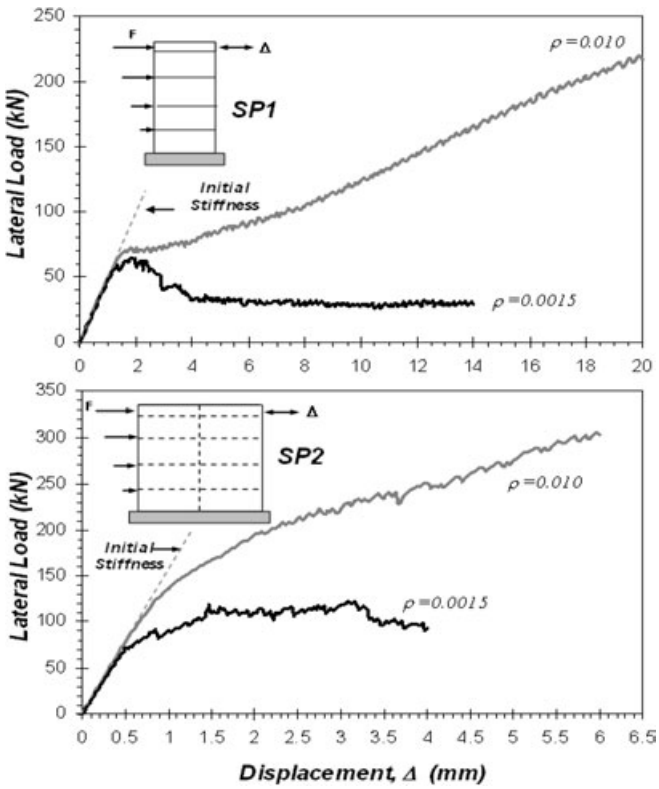

Figure 7. Capacity curve comparison for different vertical reinforcement ratio at failure. Note: abscissa and ordinates of the two figures are different

DOI: 10.1002/tal

concrete, whereas for SP2 crushing of concrete was observed before the rupture of longitudinal bars. Figures 6 and 7 collectively indicate that a higher amount of minimum tensile reinforcement is essential for ductile behavior of tunnel-form buildings, similar to cantilever walls where there is no possibility for redistribution of moments.

To augment our understanding the strength, stiffness and ductility variation at a localized level, moment–curvature (M–ϕ) analyses considering different reinforcement ratios were next conducted for the H-shape wall section. In this way, changes in strength and flexural rigidities were related to cracking and crushing of the concrete, yielding, strain hardening and rupturing of the reinforcing steel. The moment–curvature analyses were based on the strain compatibility and equilibrium of forces (Yüksel, 2003). The H-shape wall section was divided into 1 mm fiber layers, each lying parallel to the neutral axis. The following assumptions were made in the analyses: (1) strains in reinforcement and concrete were assumed to be directly proportional to the distance from the neutral axis; (2) shear lag effects in the wall flanges were ignored and total flange length was used since the flange length-to-height ratio was greater than 0·67, according to the studies by He and Priestley (1992) and Paulay and Priestley (1991); (3) axial load on the shear walls was assumed to be uniformly distributed across the entire section; (4) as the concrete strain reached its ultimate value for compression or tension at any layer, the contribution from that layer was ignored; (5) the stress–strain curve of concrete under compression was modeled according to Saatçioğlu and Ravzi (1992) and crushing was assumed to occur at an ultimate strain of 0·0038; (6) the bilinear model proposed by Rüsch and Hilsdorf (1963) was used to model the tension strength of concrete (ε_{cto} and ε_{ctu} were taken as 0·0001 and 0·0002, respectively); (7) measured stress–strain relationship of steel reinforcing bars, including strain hardening, was used in the computations (see Figure 3d).

Figure 8 compares the moment–curvature diagrams for a symmetrical flanged wall with load applied parallel (SP1) and perpendicular (SP2) to the web as the longitudinal reinforcement ratios were varied from 0·0015, 0·003 and 0·006 to 0·01. For both SP1 and SP2, when the bottom concrete strain reached the cracking strain of the concrete, the section cracked, initial stiffness changed and moment values fell sharply. In Figure 8, cracking marks the points where the moment–curvature relationship began to change its slope. The change in slope is more dramatic in SP1 than in SP2 due to wide flanges lying parallel to the section centroidal axis. The curvature and moment values corresponding to these stages are not greatly influenced due to increase in reinforcement ratio. When the moment values started to increase again, cracks were propagated through the neutral axis of the section. For SP1, when the steel strain value at the tension side flange reached the yield strain (ε_{sy} = 0·0027) of the mesh reinforcement, all reinforcement in the tension side flange yielded. For SP1, the moment curvature diagram remained almost flat beyond that point. However, for SP2, when the bottom steel strain value reached the yield strain, steel layers in the tension part of the section yielded consecutively and the moment capacities continued to increase. Therefore, this part is in rounded shape for SP2. The moment curvature diagram remains almost flat after all the web reinforcement yielded.

For SP1, when the steel strain at the tension side flange reached the ultimate steel strain value of the mesh reinforcement (ε_{su} = 0·025), all the longitudinal bars in the tension side flange ruptured simultaneously. Top concrete fiber strain values remained much lower than the crushing strain of the concrete (ε_{cu} = –0·0038) for four different reinforcement ratios (0·0015, 0·003, 0·006, 0·01). Failure mechanism of SP1 for each case was initiated due to rupturing of all the longitudinal mesh reinforcement at the tension side flanges without crushing of concrete, which eventually defines the capacity of the section. It is worth noting that the cracking moments for SP1 having reinforcement ratios of 0·0015 and 0·003 were higher than the yield and ultimate moments. However, if the reinforcement ratios were increased to 0·006 and 0·01, the yield and ultimate moments became higher than the cracking moment. For SP1, as a result of utilizing 0·003, 0·006 and 0·01 reinforcement ratios, 1·8, 3·6 and 5·7 times larger moment capacities, respectively, were obtained compared to the moment capacity of

DOI: 10.1002/tal

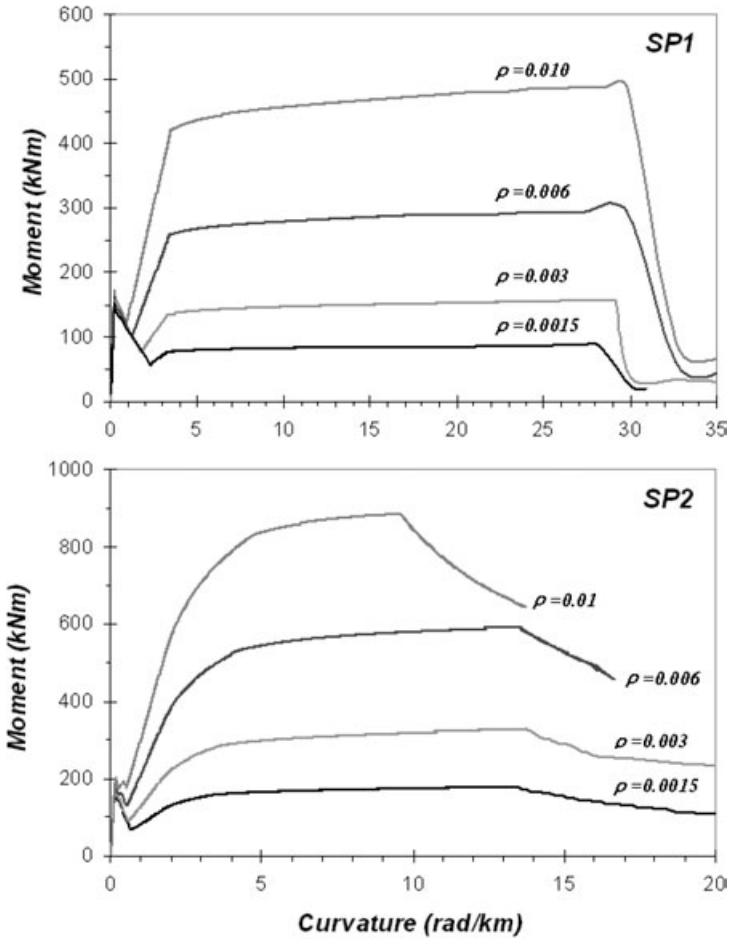

Figure 8. Variation of moment–curvature plots for SP1 and SP2 with change in shear wall reinforcement ratios. Note: ordinates of two figures are different

section with 0·0015 reinforcement ratio. By increasing the longitudinal reinforcement ratio, yield and ultimate moments increased almost linearly. However, cracking moments did not change considerably. Therefore, brittle failure due to having cracking moments greater than the yield and ultimate moments can be prevented by increasing the longitudinal reinforcement ratio.

For SP2 with reinforcement ratios of 0·0015 and 0·003, when the steel strain value at the outermost steel layers reached the rupture strain of the reinforcement steel (ε_{su} = 0·025), the longitudinal bars ruptured consecutively at the tension side of the section. The moment values then fell. For reinforcement ratios of 0·006 and 0·01, when the extreme compression fiber strain reached the crushing strain of the concrete (ε_{su} = –0·0038), the concrete fibers in the compression zones started to crush, whereas rupturing of the longitudinal reinforcement was not observed. Therefore, failure of the walls with reinforcement ratios of 0·006 and 0·01 occurred due to crushing of the concrete rather than rupturing of the reinforcement. For SP2, as a result of utilizing 0·003, 0·006 and 0·01 reinforcement ratios, 1·8, 3·3 and 4·9 times larger moment capacities were obtained compared to the moment capacity of section with 0·0015 reinforcement ratio. Similar to SP1, increasing the longitudinal reinforcement ratio, yield

DOI: 10.1002/tal

and ultimate moments increased almost linearly with no significant change in cracking moments. The cracking moment for SP2 having 0·0015 reinforcement ratio only was higher than the yield and ultimate moments.

5. EFFECTS OF BOUNDARY REINFORCEMENT ON BEHAVIOR

Boundary reinforcement for shear walls is recommended by the regulatory seismic code in Turkey for the objective of providing adequate ductility. According to provisions, boundary reinforcements should be provided at a distance of $l_b \geq 0{\cdot}2 \times l_w$ from each end of the shear wall along its critical wall height (i.e., $H_{cr} = \max[l_w, (H_w/6)]$ and H_{cr} should not be greater than $2 \times l_w$). In this additional reinforcement region, the longitudinal boundary reinforcement ratio (ρ_{bound}) should be at least 0·2% of the cross-sectional area ($2 \times b_w \times l_w$). Above the critical length (i.e., $H > H_{cr}$), boundary distance should be greater than 10% of the wall length (i.e., $l_b \geq 0{\cdot}1 \times l_w$) and longitudinal boundary reinforcement ratio (ρ_b) should be at least 0·1% of the cross-sectional area. Figure 9 illustrates the boundary reinforcement detailing recommended by TSC (1998).

In order to investigate how effective the boundary reinforcement is in enhancing the moment carrying capacity of the H-shape sections, moment–curvature analyses were employed considering two different boundary reinforcement ratios of $0{\cdot}001 \times b_w \times l_w$ (with $l_b \geq 0{\cdot}1 \times l_w$) and $0{\cdot}002 \times b_w \times l_w$ (with $l_b \geq 0{\cdot}2 \times l_w$) for SP1 and SP2 having a vertical web reinforcement ratio of 0·0015. Figures 10 and 11 demonstrate the configurations of the boundary reinforcements and compare the resultant moment–curvature curves when the section is loaded along weak and strong axes, respectively. For

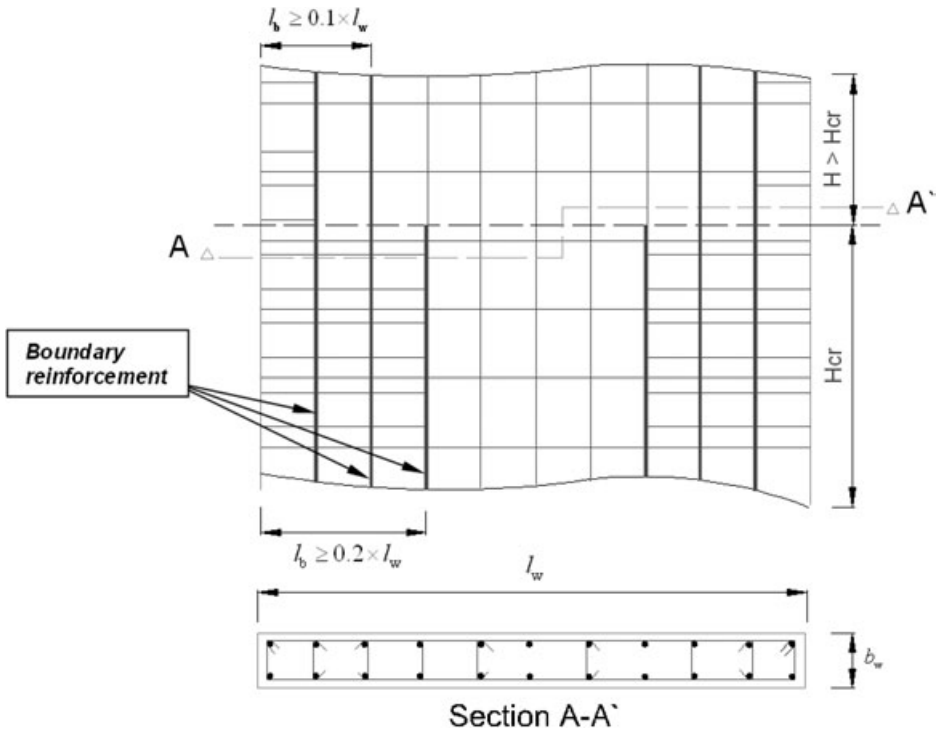

Figure 9. Detailing of boundary reinforcement in structural walls recommended by Turkish Seismic Code (TSC, 1998)

DOI: 10.1002/tal

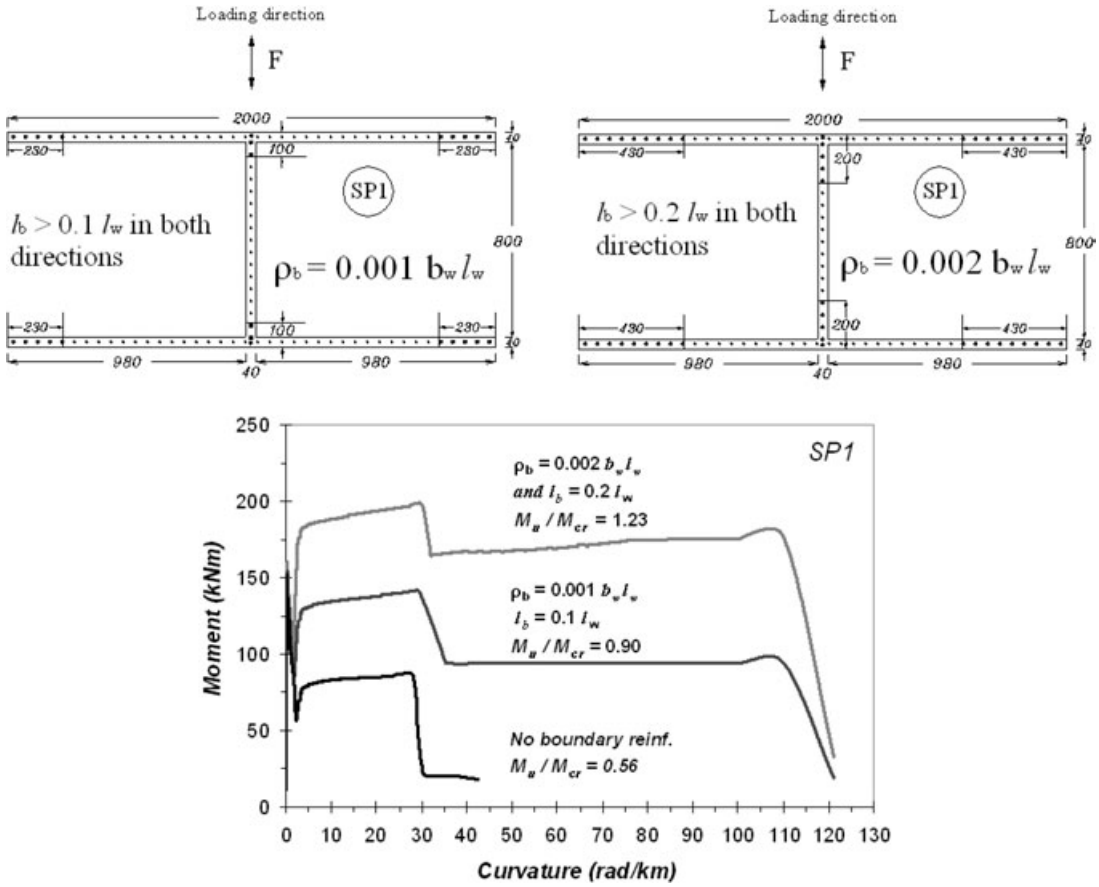

Figure 10. Comparison of moment–curvature diagrams for section with and without boundary reinforcements for loading along weak axis (SP1)

SP1 (Figure 10), placement of boundary reinforcement along both short and long dimensions significantly changed the behavior. When the strains on the mesh reinforcements along the tension flange reached their rupture values, moment capacities suddenly fell. The ultimate moment capacity reached up to 140·7 kN m and 197·7 kN m when the boundary reinforcements were placed respectively at a distance of $l_b \geq 0{\cdot}1 \times l_w$ (with ratio of $\rho_b = 0{\cdot}001 b_w l_w$) and $l_b \geq 0{\cdot}2 \times l_w$ (with ratio of $\rho_b = 0{\cdot}002 \times b_w \times l_w$). For sections having boundary reinforcement, significant differences were observed in the ratio of cracking moment capacity and ultimate moment capacity compared to sections without boundary reinforcement. A larger boundary region with a boundary reinforcement ratio of $\rho_b = 0{\cdot}002 \times b_w \times l_w$ resulted in an ultimate moment capacity 1·23 times more than the cracking moment capacity. This clearly indicates the alteration of failure mode from brittle to ductile. For a shorter confinement region with a boundary reinforcement ratio of $\rho_b = 0{\cdot}002 \times b_w \times l_w$, the ultimate moment was computed closer to the cracking moment. In this case, the failure mechanism was still brittle.

For SP2 (Figure 11), the boundary reinforcement regions were provided at a distance of $l_b \geq 0{\cdot}1 \times l_w$ and $l_b \geq 0{\cdot}2 \times l_w$, respectively, with boundary reinforcement ratios of 0·1% and 0·2% of the wall cross-sectional area in the direction of the loading. The moment–curvature curve at the top shows the

DOI: 10.1002/tal

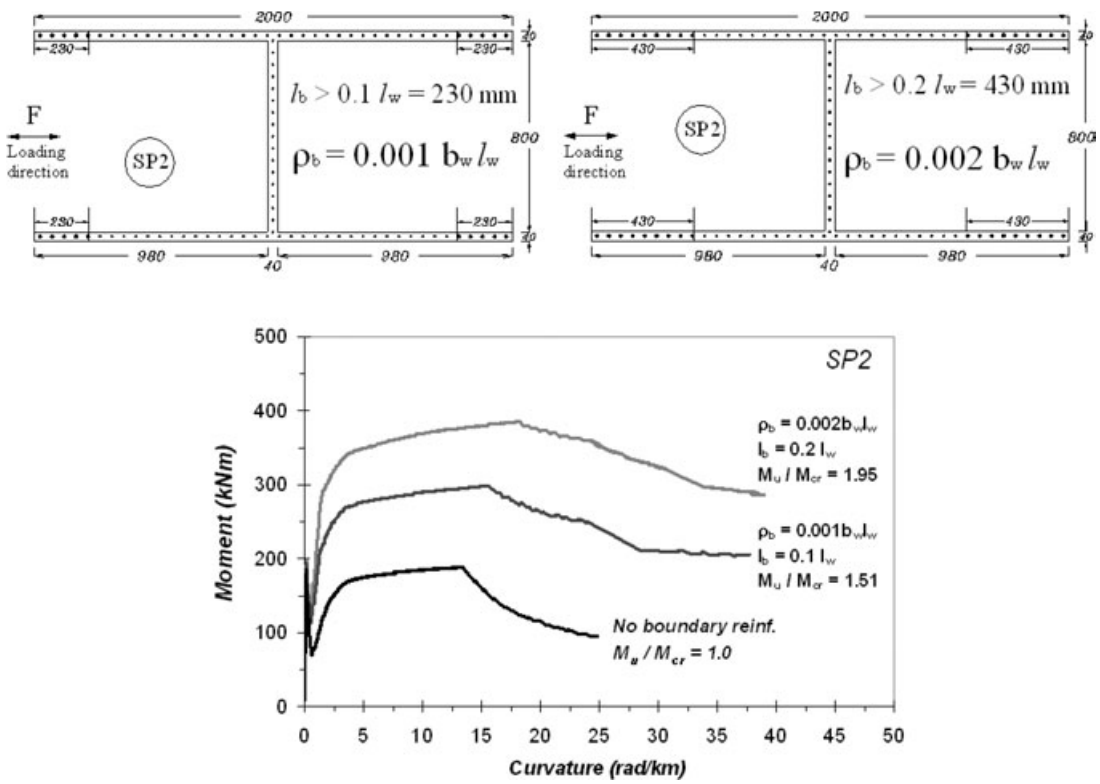

Figure 11. Comparison of moment–curvature diagrams for section with and without boundary reinforcements for loading along strong axis (SP2)

concentrated boundary reinforcement provided at a distance of $l_b \geq 0{\cdot}2 \times l_w$. In this case, the ultimate moment almost doubles the cracking moment, thereby providing significant ductility to the system when compared to sections without boundary reinforcement. By providing a larger confinement region, as the ultimate strain of the mesh reinforcement reached its rupture value, the mesh reinforcement started to rupture. In this case, the crushing of concrete was observed, in contrast to sections without boundary reinforcement.

Based on these results, it can be concluded that the additional longitudinal reinforcement used to develop confinement has significant remedial effects on behavior by establishing higher moment carrying capacity and providing larger deformation limits, as well as altering the failure mode from brittle to ductile.

6. EFFECTS OF COUPLING BEAMS AND OPENINGS ON BEHAVIOR

In tunnel-form buildings, shear walls act as primary gravity and lateral load-carrying members, and may contain openings for functional use. Wall sections above the openings of shear walls behave in a similar manner to deep coupling beams. The thickness of these beams is generally less than 250 mm for tunnel-form buildings, and much less than their counterparts in conventional RC structures. The location of shear wall openings defines the dimensions of coupling beams and their stiffness relative to shear walls, which eventually determine the portion of the overturning moments carried through axial loads in shear walls induced by vertical shears. Therefore dimensions of openings have

DOI: 10.1002/tal

significant impacts on lateral load-carrying capacity and overall rigidity of the system (see Balkaya and Kalkan, 2004b). Apparently, reducing the coupling beam section will decrease its stiffness and result in a diminishing effect on internal shear forces across the beam, yet there are generally height constraints for the coupling beams due to architectural restrictions and functional use. Therefore, elimination of high shear concentration on these coupling beams becomes a difficult design issue.

In fact, deep coupling beams with conventional reinforcement or diagonal reinforcement without confining ties are controlled by shear and do not have the desired structural properties under seismic action (e.g., Paulay 1971a, 1971b). Conventional detailing in this case consists of an equal amount of reinforcement at the top and bottom and the shear reinforcement consists of vertical stirrups with equal spacing throughout the length of the beam. Conversely, diagonally confined special reinforcements in deep coupling beams have provided adequate shear resistance (e.g., Paulay and Binney, 1974; Park and Paulay, 1975; Paulay, 1986). In recognition of the satisfactory behavior of diagonal confinement, its detailing is furnished in a number of seismic design codes (e.g., TSC, 1998; ACI 318-02, 2002; CEN, 2005). Figure 12 illustrates the typical detailing given by these provisions, whereby each diagonal element both in coupling beams and along its wall embedment should include a cage of longitudinal and transverse reinforcement and closely spaced hoops or spiral reinforcement confining the diagonal bars. This reinforcement detailing has some inherent drawbacks when applied to tunnel-form buildings due to the limited space allowed by thin shear walls. For this reason, it is generally avoided in applications (one such example is portrayed in Figure 12). Therefore, there is still a need for an innovative practical solution for avoiding high shear concentration in coupling beams of tunnel-form buildings.

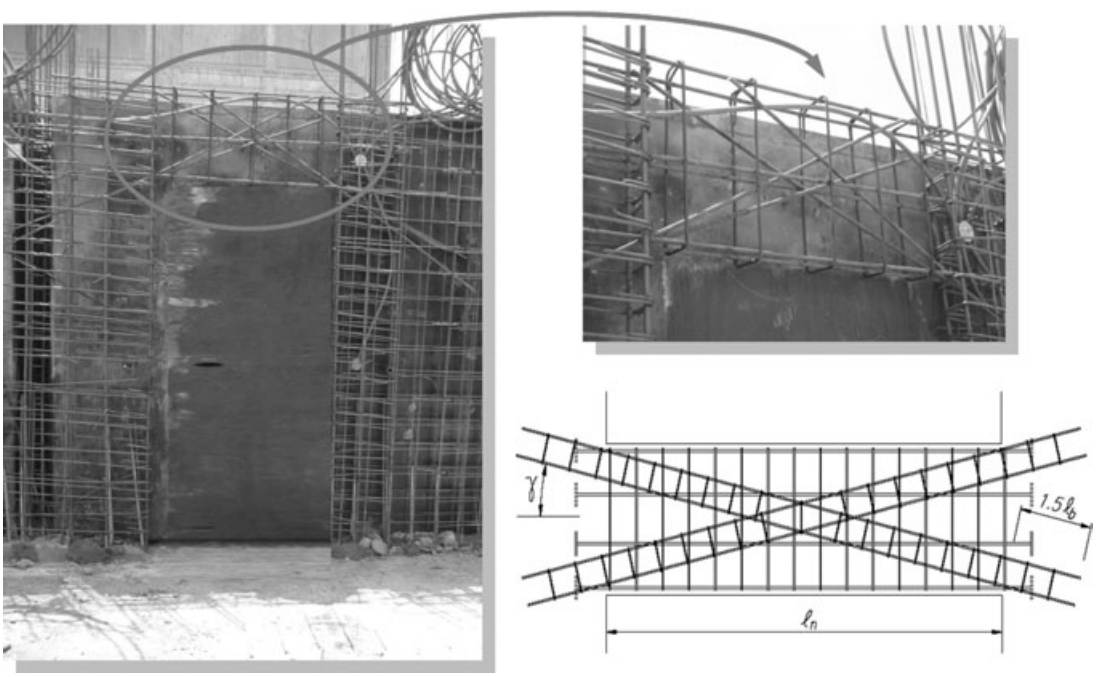

Figure 12. Comparison of reinforcement detailing for coupling beams used in practice with code-recommended detailing

DOI: 10.1002/tal

7. EFFECTS OF TENSION–COMPRESSION COUPLING ON BEHAVIOR

In tunnel-form buildings, owing to the shape of wall configurations in 3D, in-plane or membrane forces within shear walls originate a tension–compression (T/C) force couple due to combined effects of strong wall-to-wall (even including walls with openings) and wall-to-slab interactions (Balkaya and Kalkan, 2004a). In this mechanism, the outer walls oriented perpendicular to lateral loading directions act as flanges when subjected to bending loads and resist against total moment primarily in tension and compression. On the other hand, the inner walls passing from the centroid and oriented to the same direction with lateral loading act in bending, and their contribution to overall moment capacity is relatively small. In general, this 3D originated mechanism shows a characteristic T-section behavior. Therefore, the resultant force mechanism exhibits a significant contribution in the capacity and seismic performance of buildings. The basic development of the T/C coupling mechanism is illustrated in Figure 13. Previous investigations showed that in order to reflect the realistic performance of tunnel-form buildings 3D analyses should be preferred instead of 2D analyses, although the latter are commonly used in practice (Balkaya and Kalkan, 2003b). Since T/C coupling is weakly accomplished during 2D simulations with the transverse shear through coupling beams, transverse walls in 3D cases stiffen the sections by providing additional paths for shear transfer. In this case, the transverse walls provide extra resistances by substantially increasing the computed lateral load capacity (Balkaya and Kalkan, 2004b).

8. CONCLUSIONS

In order to expose the strong and weak points of tunnel-form buildings, a parametric study based on nonlinear FE analyses on the global level and moment–curvature analyses at the section level were performed. FE models were carefully calibrated to experimental data to achieve realistic simulations. Findings projected from this comprehensive study provide better insight into key behavioral aspects of tunnel-form buildings. The observations made lead to the following conclusions:

(1) The contribution of tensile stress in the concrete to the flexural capacity of the conventional beam and column members becomes small and can be neglected, since the tensile stress existing in the

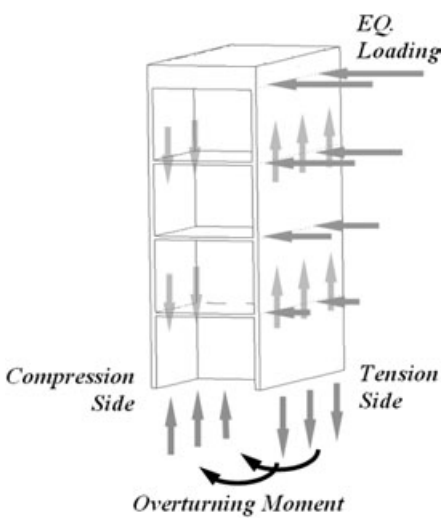

Figure 13. Initiation of global tension–compression (T/C) force couple in a typical H-shape tunnel form section

DOI: 10.1002/tal

concrete just below the neutral axis is small and has a limited lever arm. However, when the shear wall cross-section is large, as in tunnel-form buildings, the tensile strength becomes more significant. Therefore, the cracking moment of the section in some cases is even bigger than the yield and ultimate moments, suggesting that tensile resistance of concrete should be included in the calculation of the cracking moment capacity of wide-flanged shear walls.

(2) If the shear wall with very low axial load ratio is lightly reinforced with a small percentage of steel, the failure mode becomes brittle. When the tensile stress in the concrete exceeds the modulus of rupture (tensile strength), the concrete cracks and immediately releases the tensile force it carries; the lightly stressed steel should then absorb the additional load. If the area of the provided steel is too small to carry this extra force, the steel snaps and total rupture of the section occurs suddenly. If the cracking moment of a wall exceeds the ultimate moment capacity of the wall, a sudden failure occurs with little or no warning. It is therefore essential to have sufficient tensile reinforcement so that the moment capacity after cracking exceeds the cracking moment.

(3) On occasion, the construction technique of tunnel-form buildings and functional considerations may require shear wall dimensions to be set much larger than those required for flexural strength or for deflection control. Because of large lever arm between the components of the internal couple, a wall section of this type may require a very small reinforcement area. As a result, its nominal flexural strength may be less than the cracking moment of the cross-section. If the cracking moment in a wall section of this type is ever exceeded, e.g., by seismic overload, the wall may fail immediately with the rupture of the steel; a similar case was observed in the damaged eight-story El-Faro building during the 1985 Chile earthquake.

(4) Mesh reinforcement having a longitudinal and vertical steel ratio of $\rho_{sv} : \rho_{sh} = 0{\cdot}0015$ in the plane of the wall, and preventing the buckling of longitudinal bars and shear failure, is not sufficient to provide adequate ductility in both flange and web directions. The ratio of ultimate moment to cracking moment is 1·25 smaller than for a section with a reinforcement ratio as small as 0·003 when loaded in the weak direction, and a section with a reinforcement ratio of 0·0015 when loaded in the strong direction. As the reinforcement ratio decreases, the ratio of ultimate moment to the cracking moment increases. Failure occurs due to rupturing of the mesh reinforcement in the tension flange. This brittle type of behavior takes place due to under-reinforcement.

(5) An additional 0·2% unconfined boundary reinforcement placed at a distance of $l_b \geq 0{\cdot}2 \times l_w$ from each end of the wall may significantly improve the moment capacity of the section. The ultimate moment becomes larger than the cracking moment, thereby preventing brittle behavior due to under-reinforcement, and the ratio of ultimate moment to cracking moment increases.

(6) In a regular tunnel-form building, the part of the shear wall above the opening acts as a coupling beam. Such coupling beams are susceptible to high shearing forces due to dimensional constraints. Although using a code-specified diagonal layout with confining ties in these regions seems to be a reasonable solution, such detailing is generally avoided in practice due to constructional difficulties. Recently, it has been shown by Yüksel (2007) that use of slit connected coupling beams potentially reduces the high shear stress concentrations in these regions.

REFERENCES

ACI 318-02. 2002. *Building Code Requirements for Reinforced Concrete and Commentary*. ACI: Detroit, MI; 119, 234–236.

Balkaya C, Kalkan E. 2003a. Estimation of fundamental periods of shear wall dominant building structures. *Earthquake Engineering and Structural Dynamics* **32**: 985–998.

Balkaya C, Kalkan E. 2003b. Nonlinear seismic response evaluation of tunnel form building structures. *Computers and Structures* **81**: 153–165.

Balkaya C, Kalkan E. 2004a. Seismic vulnerability, behavior and design of tunnel form buildings. *Engineering Structures* **26**(14): 2081–2099.

DOI: 10.1002/tal

Balkaya C, Kalkan E. 2004b. Three-dimensional effects on openings of laterally loaded pierced shear walls. *Journal of Structural Engineering, ASCE* **130**(10): 1506–1514.
Bathe KJ. 1996. *Finite Element Procedures*. Prentice-Hall: Englewood Cliffs, NJ.
CEN. 2005. *Eurocode 8: Design of Structures for Earthquake Resistance. Part 1: European Standard*. European Committee for Standardization: Brussels.
Ghrib F, Mamedov H. 2004. Period formulas of shear wall buildings with flexible bases. *Earthquake Engineering and Structural Dynamics* **33**: 295–314.
He L, Priestley MJN. 1992. Seismic behavior of flanged masonry walls. *Structural System Research Project: Report No. SSRP-92/09*. Department of Applied Mechanics and Engineering Sciences, University of California: San Diego, CA.
Hordijk DA. 1991. Local approach to fatigue of concrete. PhD thesis, Delft University of Technology.
IBC. 2000. *International Conference of Building Officials (ICBO) 2000*. International Building Code: Whittier, CA.
Johansson M. 2000. Nonlinear finite-element analyses of concrete frame corners. *Journal of Structural Engineering, ASCE* **126**(2): 190–199.
Lee L, Chang K, Chun Y. 2004. Experimental formula for the fundamental period of RC buildings with shear wall dominant systems. *Structural Design of Tall Buildings* **9**(4): 295–307.
Park P, Paulay T. 1975. *Reinforced Concrete Structures*. Wiley: New York.
Paulay T. 1971a. Stimulated seismic loading of spandrel beams. *Journal of the Structural Division, ASCE* **97**: 2407–2419.
Paulay T. 1971b. Coupling beams of reinforced concrete shear walls. *Journal of the Structural Division, ASCE* **97**: 843–862.
Paulay T. 1986. The design of ductile reinforced concrete structural walls for earthquake resistance. *Earthquake Spectra* **2**(4): 783–823.
Paulay T, Binney JR. 1974. *Diagonally Reinforced Coupling Beams of Shear Walls: Shear in Reinforced Concrete*. Publication no. 42, American Concrete Institute: Detroit, MI.
Paulay T, Priestley MJN. 1991. *Seismic Design of Reinforced Concrete and Masonry Buildings*. Wiley: New York.
Popovics S. 1973. A numerical approach to the complete stress–strain curve for concrete. *Cement and Concrete Research* **3**(5): 583–599.
Rüsch H, Hilsdorf H. 1963. *Verformungseigenschaften von Beton Unter Zwischen Zugspannangen*. Report No. 44, Materialprüfungsamt für das Bauwesen der Technischen Hochschule München.
Saatçioğlu M, Ravzi SR. 1992. Strength and ductility of confined concrete. *Journal of Structural Engineering, ASCE* **118**(6): 1590–1607.
Takacs PF, Kanstad T. 2000. Strengthening prestressed concrete beams with carbon fiber reinforced polymer plates. *NTNU Report: R-9-00*. Trondheim, Norway.
Thorenfeldt E, Tomaszewicz A, Jensen JJ. 1987. Mechanical properties of high strength concrete and application in design. In *Proceedings of the Symposium on Utilization of High Strength Concrete*, Stavanger, Norway, June. Tapit: Trondheim; 149–159.
TNO DIANA. 2004. *TNO Building Construction and Research*. Delft, The Netherlands.
TSC. 1998. *Turkish Seismic Code (TSC1998): Specifications for the Structures to be Built in Disaster Regions*. Ministry of Public Work and Settlement: Ankara.
UBC. 1997. *International Conference of Building Officials (ICBO) 1997*. Uniform Building Code: Whittier, CA.
Wood SL, Stark R, Greer SA. 1991. Collapse of eight-story RC building during 1985 Chile earthquake. *Journal of Structural Engineering, ASCE* **117**(2): 600–619.
Yüksel SB. 2003. A moment–curvature program for structural walls. *Journal of Engineering and Architecture, Faculty of Selçuk University* **18**(1): 75–84.
Yüksel SB. 2007. Slit connected coupling beams for tunnel form building structures. *Structural Design of Tall Buildings* (in press).
Yüksel SB, Kalkan E. 2007. Behavior of tunnel form buildings under quasi-static cyclic lateral loading. *Structural Engineering and Mechanics* (in press).

DOI: 10.1002/tal